THE ASTROPHYSICAL JOURNAL, 347:96–111, 1989 December 1

THE MINIBLAZAR IN 3C 273

C. D. IMPEY
Steward Observatory, University of Arizona
M. A. MALKAN
Astronomy Department, University of California, Los Angeles
AND
S. TAPIA
Steward Observatory, University of Arizona
Received 1988 December 21; accepted 1989 May 31

ABSTRACT

The compact core in 3C 273 has been studied for over 2 years using optical photometry and accurate polarimetry. A wealth of polarization behavior is observed at a level of under 1%. Highly significant variations in the normalized Stokes parameters Q/I and U/I occur on time scales of days to years, and the changes appear stochastic on the Q/I versus U/I plane. The peak polarization is almost 2%, and the amplitude of the polarization variability increases toward longer wavelengths. Position angle rotations with wavelength are small. 3C 273 differs from other low-polarization active galactic nuclei (AGNs), which do not show large variations in the amount or orientation of linear polarization. The effects of dust scattering cannot explain the observations. A simple stochastic model with highly polarized subunits flaring and fading also fails to account for the data.

The results indicate that 3C 273 harbors a weak continuum component having all the characteristic properties of blazars. This miniblazar component ($p \sim 10\%$–20%) is probably diluted by light typical of a normal low-polarization quasar. We predict that other compact radio sources with low optical polarization ($p < 3\%$) will also be found to harbor miniblazars. In general, the detectability of optical blazar emission is a function of the compactness of the radio source. In addition to the variable component in 3C 273, a small and stable polarization of only 0.3% is seen in the ultraviolet, at position angle of $60° \pm 10°$. This quiescent polarization has a weak wavelength dependence, as in many low-polarization quasars, and is probably caused by electron scattering.

The detection of variable polarization in 3C 273 strengthens the link between superluminal motion at radio wavelengths and blazar activity at optical wavelengths. At the time of maximum nuclear polarization, the position angle represents a magnetic field perpendicular to the jet axis. The location of the quiescent ultraviolet polarization is uncertain, but may arise from an accretion disk close to the power source. The miniblazar in 3C 273 lends support to the "unified" beaming models with both a beamed and an isotropic component for the optical and radio emission.

Subject headings: BL Lacertae objects — galaxies: nuclei — polarization — quasars — radio sources: variable

I. INTRODUCTION

The clearest evidence for nonthermal radiation in active galactic nuclei (AGNs) is seen in the small class of radio sources called "blazars." Following Angel and Stockman (1980), we define blazars as AGNs with compact radio emission, rapid and large-amplitude variability, and a high degree of linear polarization at optical and infrared wavelengths. High polarization is almost always associated with flux variability and compact radio emission (Moore and Stockman 1984). There are a few AGNs with high polarization due to scattering rather than synchrotron emission, but these sources do not have compact radio cores and variable polarization (Angel and Stockman 1980; Wardle, Moore, and Angel 1984). The term "blazar" includes highly polarized quasars (Moore and Stockman 1981), as well as the weak-lined BL Lacertae objects. Variable polarization arises from optically thin synchrotron emission in an ordered magnetic field. The energy distributions of blazars are often strikingly simple, consistent with one smoothly curving synchrotron component from 10^{11} to 10^{14} Hz (Landau *et al.* 1986; Impey and Neugebauer 1988).

Indirect arguments for bulk relativistic motion in the emission regions of blazars include luminosities that exceed the Eddington limit for spherical accretion onto a compact source (Impey *et al.* 1982), radio brightness temperatures that exceed the limit for synchrotron emission (Condon and Dennison 1978), and an absence of the strong X-ray emission that is expected from Compton scattering of millimeter photons (Madejski and Schwartz 1983). At least 70% of the confirmed superluminal radio sources have blazar properties (Impey 1987). The apparent superluminal motion of VLBI components is strong evidence for relativistic motion along a trajectory close to the line of sight.

Relativistic motion may be common among AGNs. The kinematic boosting of apparent flux density is large when the beam is aligned near the line of sight. Therefore, in a flux-limited survey of a beamed property, such as compact radio emission, sources with beams near the line of sight will be overrepresented (Blandford and Rees 1978). Also, there will be a large number of misaligned sources for every beamed source (Urry and Shafer 1984). The category of models where the observed properties of an AGN depend on the orientation are called "unified" schemes. The validity of simple unified models is still being debated (Barthel 1988; Browne and Murphy 1987; Peacock 1986), but it is important to pursue these ideas. AGN research is burdened with observational classifications and morphological distinctions, yet geometric effects may account for many of the apparent differences between types of AGNs (e.g., Browne 1983; Antonucci and Miller 1985).

Complete radio samples have been used to study the connection between compact radio emission, superluminal motion, and blazar properties. New VLBI studies have shown that a large fraction of compact radio sources show superluminal motion (Pearson and Readhead 1988). Also, Impey and Tapia (1988) have found that ~40% of a complete sample of 5 GHz radio sources have high optical polarization, and that the fraction increases with radio compactness. Given these relationships, 3C 273 is enigmatic. This well-known quasar (1226+023, $V = 12.9$, $z = 0.158$) has a compact radio core, a jet visible at radio and optical wavelengths, and VLBI components which display relativistic motion (Unwin *et al.* 1985). Yet the optical and near-infrared flux is mostly quiescent (Neugebauer *et al.* 1979; Gear *et al.* 1984), while the linear polarization never exceeds 3% (Stockman, Moore, and Angel 1984; Smith *et al.* 1987; Courvoisier *et al.* 1988). Here we present the results of optical photometry and polarimetry to search for blazar activity in 3C 273.

II. OBSERVATIONS

a) Calibration of the Instrument

The observations were made with the MINIPOL polarimeter at the Las Campanas Observatory in Chile, on the 100 inch (2.5 m) (Du Pont) and 40 inch (1 m) telescopes. Polarimetry and photometry of 3C 273 were acquired in six separate runs during the period 1984 March to 1986 June. A journal of observations is given in Table 1, with the telescope, dates, filters used, and apertures used listed in columns (1)–(4). The observations were acquired during clear and photometric weather, with seeing in the range of 0″.7 to 2″.5, and a median image diameter of 1″.2. Measurements of 3C 273 were limited by photon statistics.

MINIPOL uses a Wollaston prism and two GaAs tubes for high throughput. A superachromatic half-wave plate rotates through a full modulation cycle in 12 ms. The characteristics of the instrument are described by Dolan and Tapia (1986). The sensitivity of MINIPOL in photon flux units has been calibrated over the entire GaAs wavelength range. The five spectral bands of the polarimeter approximate the *UBVRI* system, and the effective wavelengths, after convolving the instrumental sensitivity (GaAs tubes) and filter transmission with the 3C 273 energy distribution (from de Bruyn and Sargent 1978), are 3579 Å(U), 4461 Å(B), 5378 Å(V), 6860 Å(R), and 7878 Å(I). The discrete sampling of the modulator leads to polarization efficiency correction factors of 1.0294 (U), 1.0217 (B), 1.0167 (V), 1.0137 (R), and 1.0159 (I). The normal observing sequence was M seconds of object integration followed by N seconds of background integration on a blank patch of sky about 30″ away. To reduce the statistical error of the background observation, the ratio of N to M was kept less than the square root of the ratio of counts from the sky background to counts from the object (Young 1974).

The zero point for the position angle of polarization was calibrated using a Glan-Thompson prism, as described in Dolan and Tapia (1986). Two polarization standard stars were frequently observed. Table 2 presents the mean linear polarization, position angle, and standard deviation of 20 measurements of HD 147889 (Bailey and Hough 1982) made at the 100 inch (2.5 m) telescope, and 17 measurements of HD 110984 made at the 100 (2.5 m) and 40 inch (1 m) telescopes. Along with other stars, the results for HD 110984 have been used to establish polarimetric standard stars for the Hubble space telescope (Tapia 1988). The standard star polarimetry is shown in Figure 1, and it clearly shows the repeatability of MINIPOL measurements over a period of years. Integration times on standard stars were typically short, 1 minute or less. Figure 2 shows the polarization error as a function of total counts for measurements of HD 147889 (*filled circles*) and 3C 273 (*crosses*). Two conclusions can be drawn from the data in Figure 2. First, the polarization error reduces according to photon-counting statistics. In other words, the observed error from the fit to the modulated signal agrees with the predicted polarization error, $100(2/N)^{1/2}$, where N is the number of counts. Second, the long integrations on 3C 273 yielded a large number of total counts, giving a polarization precision in most cases of better than 0.1%.

b) Photometry

The *UBVRI* magnitudes were calibrated with nightly observations of the bright photometric standard stars HD 47761, HD 147889, HD 149382, and L99-408 (Landolt 1973). Magnitudes of these standards, derived with the 2″.7 aperture at the 100 inch (2.5 m) and the 3″.8 aperture at the 40 inch (1 m), have an rms of 0.08–0.12 mag. Additional photometry obtained at the 100 inch (2.5 m) with the 5″.3 and 8″.0 apertures shows variations of rms 0.04–0.06 mag. The same range of variation is detected in the night-to-night comparison of the photometry and may be caused by electronic drift. Most of the observations were made at small air mass, and, after a preliminary check for consistency, the standard CTIO extinction coefficients were applied. Except for observations in the U band with the 2″.7 aperture, the effects of differential refraction were very small, in agreement with Fillipenko (1982), who found that the differential refraction from the U to the R band is only 0″.7 at 1.2 air mass.

TABLE 1

JOURNAL OF OBSERVATIONS

Telescope (1)	Dates (UT) (2)	Filters (3)	Apertures (4)
Las Campanas 100 inch (2.5 m) ...	84/03/22–84/04/02 (A)	U, B, V, R, I	2″.7, 5″.3, 8″
Las Campanas 40 inch (1 m)	84/04/05–84/04/10 (B)	U, V, I	3.8
Las Campanas 40 inch (1 m)	85/01/15–85/01/16 (C)	U, V, I	3.8
Las Campanas 100 inch (2.5 m) ...	85/01/24–84/02/07 (D)	U, V, I	2.7, 8
Las Campanas 100 inch (2.5 m) ...	85/04/10–85/04/16 (E)	U, V, I	2.7
Las Campanas 100 inch (2.5 m) ...	86/05/31–86/06/04 (F)	U, V, I	2.7, 5.3

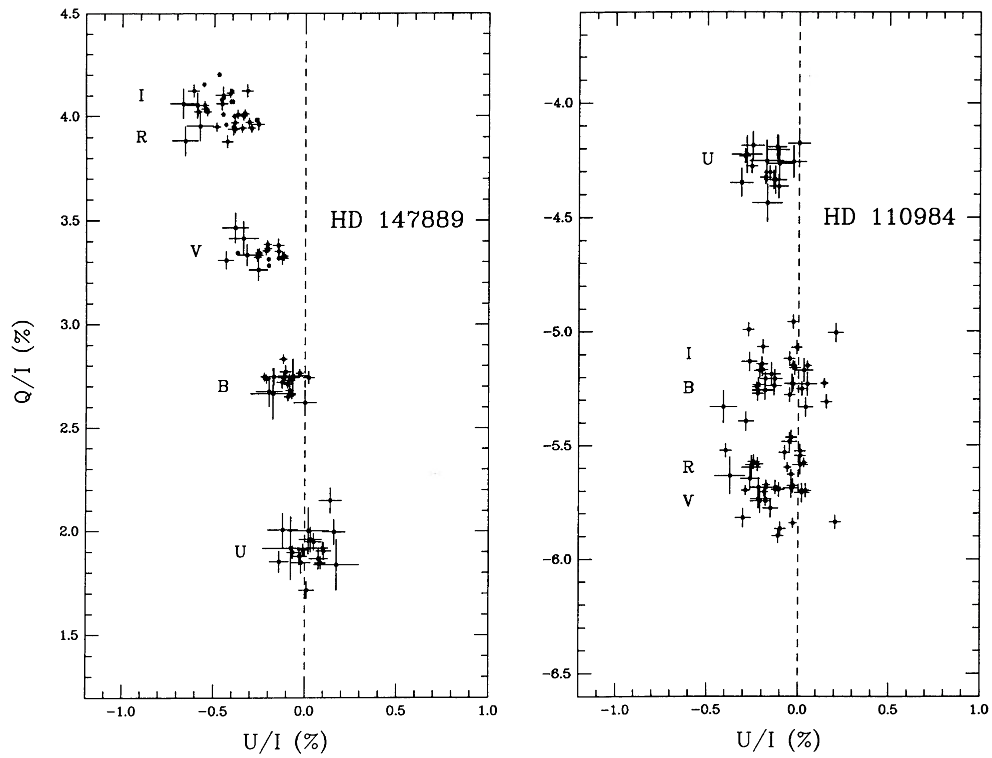

FIG. 1.—Normalized Stokes parameters (in percent) plotted for the standard stars (*a*) HD 147889 and (*b*) HD 110984

In addition to photometric standard stars, we monitored the brightness of four field stars near 3C 273, identified by Smith *et al.* (1985) as stars *B*, *D*, and *G* (with a few measurements of star *E*). The 1 σ scatter in the *U* and *V* magnitudes for stars *B*, *D*, and *G* is 0.06 mag. This is similar to the scatter in standard star photometry and gives a good estimate of the night-to-night photometric reliability of measurements through a large aperture. The average *U* and *V* magnitudes for the field stars agree with those reported previously to better than 0.05 mag (Burkhead 1969, 1980; Smith *et al.* 1985). Thus, our absolute photometric calibrations at *U* and *V* are good to this level. The photometry is presented in Table 3, with the UT date and telescope used for the observations in columns (1) and (2), and the aperture size in arcseconds and magnitude for the five filters in columns (3)–(12). Observations with uncertainties larger than 0.1 mag are marked with a dagger. The larger errors are mostly due to seeing and guiding corrections for observations in the *U* band or the smallest aperture. Seeing losses do not depend on wavelength, so the *colors* measured in the 2″7 aperture are better determined than the magnitudes. Thus the agreement from night to night of standard star $V-I$ colors measured in the small aperture is 0.03 mag (1 σ).

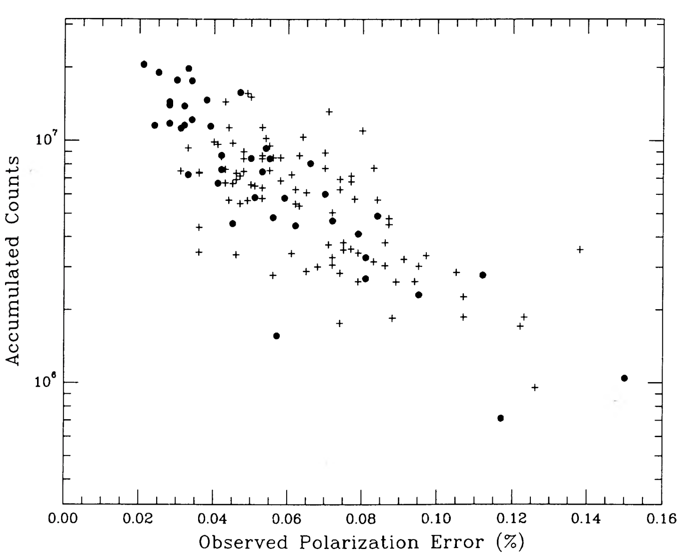

FIG. 2.—Accumulated counts plotted against polarization error for observations of the standard star HD 147889 (*filled circles*) and 3C 273 (*crosses*).

The photometry reveals no large change in the brightness of the optical continuum of 3C 273, even during a dramatic increase in the polarization. The peak of the polarization outburst was on the nights of 1984 March 24 and 25 (UT). On these two nights, 3C 273 was brighter than on the remaining nights of the March run, by 0.09 mag at *I*, 0.11 mag at *V*, and 0.03 mag at *B* (with no change at *U*). On March 24, 3C 273 was observed to be 0.07 mag brighter than field star *G*, compared with 0.06 ± 0.01 mag brighter for the average of five sub-

TABLE 2

POLARIZATION STANDARDS: HD 147889 AND HD 110984

Filter (1)	HD 147889 $p \pm \sigma(p)$ (2)	HD 147889 $\theta + \sigma(\theta)$ (3)	HD 110984 $p \pm \sigma(p)$ (4)	HD 110984 $\theta + \sigma(\theta)$ (5)
U	2.04% ± 0.26%	180°5 ± 3°5	4.35% ± 0.01%	92°3 ± 0°1
B	2.74 ± 0.10	178.8 ± 1.0	5.31 ± 0.01	92.0 ± 0.1
V	3.32 ± 0.06	177.6 ± 0.5	5.70 ± 0.01	91.6 ± 0.1
R	3.97 ± 0.07	176.7 ± 0.5	5.67 ± 0.01	91.2 ± 0.1
I	4.08 ± 0.05	176.5 ± 0.3	5.17 ± 0.01	90.8 ± 0.1

TABLE 3

3C 273 PHOTOMETRY

U.T. Date	Telescope	U		B		V		R		I	
		Aper	Mag	Aper	Mag	Aper	Mag	Aper	Mag	Aper	Mag
(1)	(2)	(3)	(4)	(5)	(6)	(7)	(8)	(9)	(10)	(11)	(12)
3/22/84	100	...	...	...	...	5.3	13.03	5.3	12.72	5.3	11.96
3/23/84	100	2.7	12.39†	2.7	13.18	2.7	12.81	...	...	5.3	11.87
3/24/84	100	2.7	12.04	...	...	2.7	12.83	...	...	2.7	11.86
3/25/84	100	5.3	12.12	2.7	13.28	5.3	13.01	2.7	12.83	...	...
3/26/84	100	8.0	12.09	2.7	13.09	8.0	12.91	...	...	2.7	11.97
3/27/84	100	8.0	12.08	...	...	8.0	12.87	...	...	2.7	11.96
3/28/84	100	8.0	12.19	...	...	8.0	12.96	...	...	2.7	11.97
3/29/84	100	2.7	12.11	2.7	13.13	2.7	12.88	...	...	2.7	11.93
4/01/84	100	8.0	12.06	...	...	8.0	12.86	...	...	2.7	12.04†
4/02/84	100	2.7	12.36†	...	...	2.7	12.92	2.7	12.73	2.7	11.95
4/05/84	40	3.8	12.37	...	...	3.8	12.97	...	...	3.8	11.98
4/06/84	40	3.8	12.21	...	...	3.8	13.09	...	...	3.8	12.10
4/07/84	40	3.8	12.28	...	...	3.8	12.97	...	...	3.8	12.02
4/08/84	40	3.8	12.31	...	...	3.8	12.93	...	...	3.8	11.99
4/09/84	40	3.8	12.33	...	...	3.8	13.09	...	...	3.8	12.07
4/10/84	40	3.8	12.45	...	...	...	...	...	...	3.8	12.01
1/16/85	40	3.8	...	...	...	...	...	...	...	3.8	12.20†
1/17/85	40	...	...	...	...	3.8	13.02†	...	...	3.8	12.36†
1/24/85	100	8.0	12.16	...	...	8.0	12.78	...	...	2.7	12.02
1/25/85	100	...	...	...	...	...	...	...	...	2.7	11.97
1/29/85	100	8.0	12.16	...	...	8.0	12.79	...	...	2.7	12.16
1/30/85	100	...	...	...	...	2.7	12.79	...	...	2.7	11.94
1/31/85	100	...	...	...	...	2.7	12.80	...	...	2.7	12.08
2/01/85	100	...	...	...	...	...	...	...	...	2.7	11.89
2/04/85	100	...	...	...	...	...	...	...	...	2.7	11.93
2/05/85	100	...	...	...	...	...	...	...	...	2.7	11.89
2/06/85	100	...	...	...	...	2.7	12.85	...	...	...	...
2/07/85	100	...	...	...	...	2.7	12.83	...	...	2.7	11.88
4/10/85	100	...	...	...	...	2.7	12.79	...	...	2.7	12.07
4/11/85	100	...	...	...	...	...	...	...	...	2.7	11.99
4/13/85	100	...	...	...	...	...	...	...	...	2.7	11.92
4/14/85	100	...	...	...	...	2.7	12.69	...	...	2.7	11.88
4/16/85	100	...	...	...	...	...	...	...	...	2.7	11.94
5/31/86	100	5.3	12.31†	...	...	5.3	13.08†	...	...	5.3	12.48†
6/01/86	100	2.7	12.24†	...	...	2.7	13.04†	...	...	2.7	11.97†
6/02/86	100	2.7	12.09†	...	...	2.7	12.71†	...	...	2.7	11.88†
6/03/86	100	2.7	12.04†	...	...	2.7	12.71†	...	...	2.7	11.98†
6/04/86	100	2.7	12.40†	...	...	2.7	12.80†	...	...	2.7	12.13†

NOTE.—Measurements through 5″.3 or 8″ apertures accurate to 0.04–0.06 mag. Measurements through 2″.7 aperture accurate to 0.08–0.12 mag. Measurements marked with a dagger have uncertainties larger than 0.10 mag.

sequent nights. This is independent support for a lack of variability. The variations in I magnitude and $V-I$ color during the flare are plotted in Figures 3*a* and 3*c*. The optical activity was matched by infrared variability. Courvoisier *et al.* (1987) found 3C 273 to be in a moderately bright state on 1984 January 28 and April 18. On March 21, relative to this level, 3C 273 was brighter by 9% at 1.2 μm, 9% at 1.6 μm, and 14% at 2.2 μm. However, the optical spectrum did *not* become significantly redder at the peak of the polarization burst on March 24 and 25. Our $V-I$ colors show 3C 273 to be slightly *bluer* on those nights. Its $V-I$ color could not have been redder by more than 0.08 mag (2 σ), relative to the rest of the March run. Therefore, we confirm the results of photoelectric measurements over the last two decades (Burkhead 1969, 1980; Burkhead and Lee 1972; Burkhead and Rettig 1972; Courvoisier *et al.* 1987). 3C 273 is variable on time scales as short as 1 day, but the duty cycle of variability above the 10% level is very long.

c) Polarimetry

Although MINIPOL delivers simultaneous photometry and polarimetry, when the aperture size approaches the diameter of the seeing disk, the result is accurate polarimetry but poor photometry. The accuracy of the polarimetry is preserved because MINIPOL registers the values of the normalized Stokes parameters Q/I and U/I, with a sampling frequency of 83.3 Hz. This modulation is fast enough to be virtually unaf-

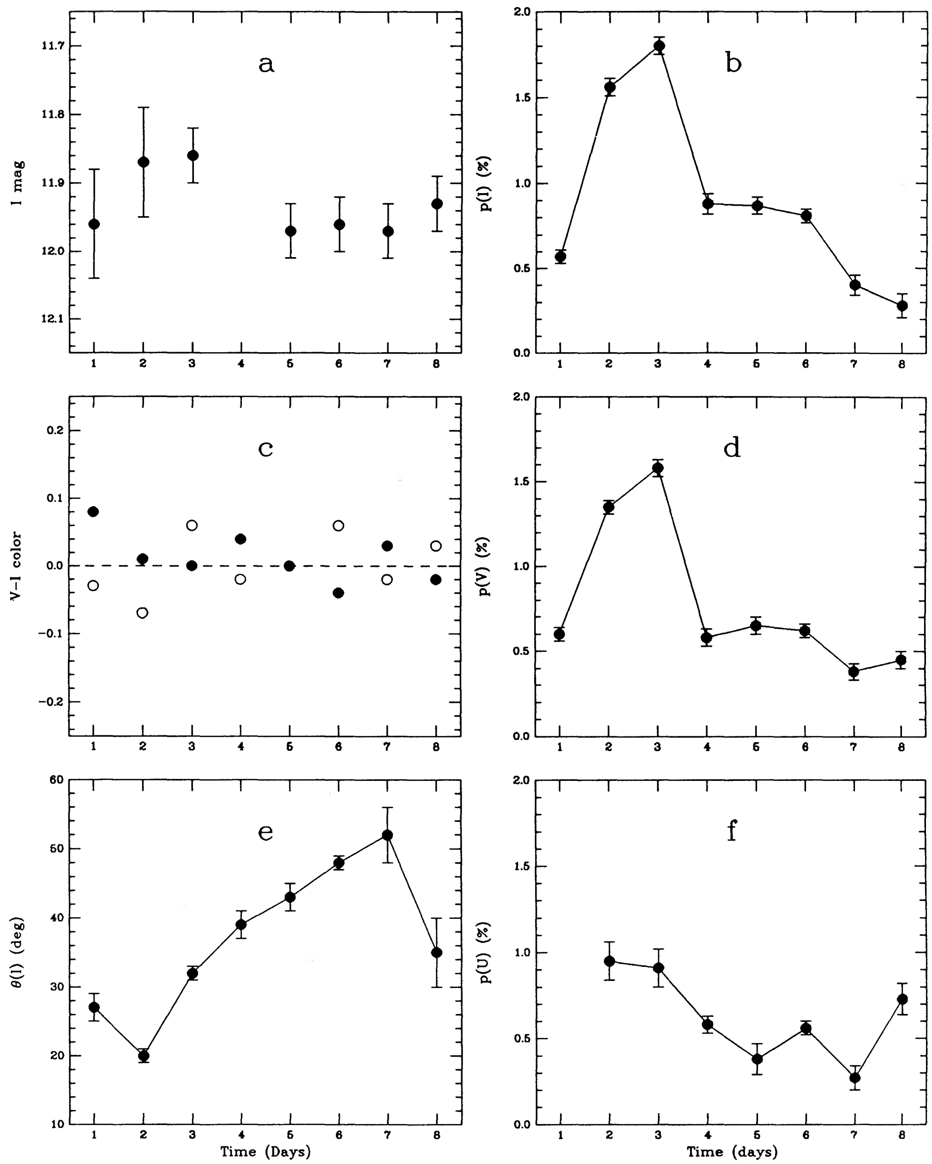

FIG. 3.—Data from the 1984 March flare event, separated into (*a*) *I* magnitude, (*b*) *I*-band polarization, (*c*) $V-I$ color (*filled circles*, 3C 273; *open circles*, standard stars), (*d*) *V*-band polarization, (*e*) *I*-band polarization position angle, and (*f*) *U*-band polarization. Day 1 is 1984 March 22 UT.

fected by light losses due to variable seeing (Serkowski 1974). All the polarization measurements of 3C 273 were made using the 2".7 aperture at the 100 inch (2.5 m), and the 3".8 aperture at the 40 inch (1 m) telescope. The apertures of MINIPOL are bored in Mylar, and light scattering off the edge of these apertures should be free from instrumental polarization. To confirm this, a faint BL Lacertae object was observed through small and large apertures for 16 minutes per wave band. The results presented in Table 4 indicate a negligible difference between the two sets of observations. The apertures used are small enough that the optical flux is dominated by nuclear emission, with a negligible contribution from the extended 3C 273 jet.

Table 5 lists 112 polarization observations of 3C 273, taken on 41 different nights and through five different filters. Column (1) gives the UT date of the observation, and column (2) gives the filter. The integration time on the source in minutes is listed in column (3). The unbiased percent of polarization and the 95% confidence interval are presented in columns (4) and (5), where $p = ([Q/I]^2 + [U/I]^2)^{1/2}$. The position angle and associated error are in columns (6) and (7), where $\theta =$

TABLE 4

POLARIZATION MULTIAPERTURE TEST: 0754+101

	APERTURE = 2".7		APERTURE = 16".2	
FILTER (1)	$p \pm \sigma(p)$ (2)	$\theta \pm \sigma(\theta)$ (3)	$p \pm \sigma(p)$ (4)	$\theta \pm \sigma(\theta)$ (5)
U	16.7% ± 1.0%	37° ± 2°	15.9% ± 1.0%	38° ± 2°
B	16.0 ± 0.5	38 ± 1	16.2 ± 0.6	38 ± 1
V	15.5 ± 0.6	38 ± 1	16.2 ± 0.8	39 ± 1
R	15.8 ± 0.3	39 ± 1	14.9 ± 0.7	40 ± 1
I	14.7 ± 0.7	37 ± 1	15.4 ± 0.8	36 ± 1

TABLE 5

3C 273 POLARIMETRY

U.T. Date (1)	Filter (2)	Time (min) (3)	p (%) (4)	σ(p) (95% conf) (5)	θ (deg) (6)	$\sigma(\theta)$ (deg) (7)	Q/I (8)	U/I (9)	σ(Q/I) (10)	Aper. (arcsec) (11)	C_1 (12)	C_2 (13)
3/22/84	I	36	0.57	0.49/0.65	27	2	+0.47	+0.41	0.04	5.3	0.5	0.02
3/22/84	R	36	0.54	0.44/0.64	30	3	+0.42	+0.41	0.05	5.3	0.3	0.04 †
3/22/84	V	36	0.60	0.52/0.68	34	2	+0.39	+0.49	0.04	5.3	0.1	0.03 †
3/23/84	I	22	1.56	1.46/1.66	20	1	+1.34	+0.95	0.05	2.7	12.9	0.01
3/23/84	V	32	1.35	1.27/1.43	25	1	+1.03	+0.97	0.04	2.7	3.7	0.01
3/23/84	B	18	1.12	0.95/1.27	21	2	+0.99	+0.69	0.08	2.7	1.4	0.02
3/23/84	U	24	0.95	0.72/1.17	34	3	+0.49	+0.84	0.11	2.7	1.0	0.03
3/24/84	I	12	1.80	1.70/1.90	32	1	+0.93	+1.56	0.05	2.7	68.2	0.01
3/24/84	V	12	1.58	1.48/1.68	30	1	+0.96	+1.31	0.05	2.7	8.6	0.01
3/24/84	U	12	0.91	0.68/1.13	32	3	+0.54	+0.78	0.11	2.7	9.0	0.01
3/25/84	I	18	0.88	0.76/1.00	39	2	+0.32	+0.81	0.06	2.7	14.4	0.01
3/25/84	R	18	0.63	0.48/0.76	44	3	+0.18	+0.57	0.07	2.7	7.2	0.02
3/25/84	V	18	0.58	0.49/0.67	37	3	+0.32	+0.50	0.05	2.7	5.9	0.01
3/25/84	B	18	0.62	0.52/0.72	51	2	+0.03	+0.55	0.05	2.7	2.5	0.02
3/25/84	U	24	0.58	0.48/0.68	59	3	−0.14	+0.46	0.05	2.7	4.8	0.02
3/26/84	I	16	0.87	0.77/0.97	43	2	+0.20	+0.82	0.05	2.7	7.4	0.02
3/26/84	V	24	0.65	0.55/0.75	42	2	+0.23	+0.59	0.05	2.7	17.0	0.02
3/26/84	B	16	0.70	0.53/0.85	47	3	+0.11	+0.64	0.08	2.7	22.3	0.02
3/26/84	U	30	0.38	0.19/0.55	51	7	+0.05	+0.33	0.09	2.7	33.3	0.03
3/27/84	I	24	0.81	0.73/0.89	48	1	+0.05	+0.76	0.04	2.7	6.5	0.02
3/27/84	V	24	0.62	0.54/0.70	50	2	+0.06	+0.55	0.04	2.7	10.6	0.01
3/27/84	U	24	0.56	0.48/0.64	52	2	−0.00	+0.49	0.04	2.7	38.3	0.02
3/28/84	I	24	0.40	0.27/0.51	52	4	+0.04	+0.33	0.06	2.7	2.0	0.05
3/28/84	V	24	0.38	0.27/0.48	70	4	−0.12	+0.18	0.05	2.7	6.3	0.03
3/28/84	B	24	0.48	0.34/0.62	70	4	−0.22	+0.25	0.07	2.7	20.1	0.01
3/28/84	U	32	0.27	0.12/0.40	95	7	−0.15	−0.10	0.07	2.7	26.3	0.05
3/29/84	I	24	0.28	0.17/0.37	35	5	+0.24	+0.22	0.05	2.7	3.4	0.05
3/29/84	V	22	0.45	0.34/0.54	46	3	+0.15	+0.39	0.05	2.7	11.0	0.01
3/29/84	B	12	0.56	0.40/0.72	38	4	+0.30	+0.49	0.08	2.7	31.6	0.01
3/29/84	U	30	0.73	0.55/0.91	37	4	+0.34	+0.66	0.09	2.7	99.0	0.01
3/30/84	U	22	0.27	0.10/0.43	68	8	−0.07	+0.15	0.08	2.7	22.0	0.05
4/01/84	I	24	0.42	0.34/0.50	80	3	−0.25	+0.09	0.04	2.7	2.8	0.02
4/01/84	V	18	0.49	0.38/0.58	79	3	−0.29	+0.12	0.05	2.7	7.0	0.02
4/01/84	U	30	0.32	0.15/0.47	70	7	−0.12	+0.16	0.08	2.7	28.9	0.03
4/02/84	I	16	0.64	0.56/0.72	33	2	+0.40	+0.53	0.04	2.7	4.3	0.02
4/02/84	R	16	0.42	0.29/0.56	38	4	+0.26	+0.36	0.07	2.7	5.9	0.02
4/02/84	V	16	0.45	0.34/0.54	51	3	+0.07	+0.38	0.05	2.7	8.6	0.02
4/02/84	U	24	0.65	0.44/0.85	55	4	−0.09	+0.57	0.10	2.7	42.3	0.01
4/05/84	I	42	0.13	0.00/0.27	53	15	+0.10	+0.09	0.08	3.8	1.9	0.19
4/05/84	V	42	0.46	0.32/0.60	62	4	−0.10	+0.33	0.07	3.8	17.0	0.05
4/05/84	U	66	0.45	0.20/0.68	62	7	−0.13	+0.34	0.12	3.8	28.0	0.09
4/06/84	I	46	0.38	0.23/0.52	68	5	−0.14	+0.22	0.07	3.8	21.2	0.08
4/06/84	V	58	0.30	0.00/0.54	60	13	+0.00	+0.22	0.14	3.8	7.8	0.05
4/06/84	U	86	0.46	0.10/0.78	35	10	+0.30	+0.41	0.17	3.8	17.1	0.09
4/07/84	I	32	0.56	0.44/0.67	58	3	−0.11	+0.45	0.06	3.8	50.2	0.07
4/07/84	V	50	0.58	0.42/0.75	68	4	−0.26	+0.35	0.08	3.8	12.5	0.03
4/07/84	U	74	0.49	0.26/0.70	78	6	−0.32	+0.15	0.11	3.8	7.9	0.07
4/08/84	I	48	0.40	0.32/0.48	60	3	−0.06	+0.29	0.04	3.8	1.8	0.08
4/08/84	V	88	0.50	0.37/0.61	57	4	−0.04	+0.39	0.06	3.8	5.1	0.02
4/08/84	U	66	0.38	0.17/0.57	55	8	+0.00	+0.31	0.10	3.8	6.4	0.06
4/09/84	I	90	0.57	0.41/0.74	55	4	−0.06	+0.49	0.08	3.8	1.9	0.08
4/09/84	V	46	0.63	0.48/0.76	56	3	−0.07	+0.52	0.07	3.8	8.7	0.04
4/09/84	U	72	0.52	0.35/0.69	61	5	−0.15	+0.40	0.09	3.8	17.0	0.07
4/10/84	I	74	0.43	0.29/0.57	58	5	−0.05	+0.34	0.07	3.8	0.8	0.06
4/10/84	U	72	0.34	0.00/0.61	56	11	−0.01	+0.29	0.14	3.8	3.9	0.09

TABLE 5—*Continued*

U.T. Date (1)	Filter (2)	Time (min) (3)	p (%) (4)	σ(p) (95% conf) (5)	θ (deg) (6)	σ(θ) (deg) (7)	Q/I (8)	U/I (9)	σ(Q/I) (10)	Aper. (arcsec) (11)	C_1 (12)	C_2 (13)	
1/15/85	I	36	0.11	0.00/0.33	99	20	−0.03	−0.11	0.13	3.8	1.2	0.23	†
1/15/85	V	16	0.31	0.00/0.60	70	13	−0.10	+0.16	0.17	3.8	1.9	0.09	
1/15/85	U	42	0.71	0.33/1.05	87	8	−0.60	+0.03	0.18	3.8	4.3	0.12	
1/16/85	V	6	3.59	3.04/4.12	174	2	3.69	−0.81	0.27	22.5	0.7	0.03	
1/16/85	I	36	0.00	0.00/0.00	...	...	+0.08	−0.13	0.11	3.8	0.5	0.38	†
1/16/85	U	10	0.76	0.27/1.21	64	8	−0.36	+0.57	0.23	3.8	53.0	0.11	
1/24/85	I	16	0.21	0.12/0.28	101	5	−0.06	−0.13	0.04	2.7	2.1	0.04	
1/24/85	V	24	0.19	0.12/0.24	71	4	+0.01	+0.06	0.03	2.7	10.4	0.04	
1/24/85	U	24	0.44	0.30/0.58	68	4	−0.19	+0.26	0.07	2.7	53.0	0.01	
1/25/85	I	20	0.11	0.00/0.24	65	11	+0.05	+0.05	0.07	2.7	0.6	0.07	†
1/25/85	U	24	0.53	0.40/0.64	64	3	−0.19	+0.37	0.06	2.7	41.5	0.01	
1/29/85	I	36	0.59	0.46/0.70	116	3	−0.22	−0.52	0.06	2.7	2.8	0.04	
1/29/85	V	24	0.38	0.25/0.49	86	4	−0.21	−0.01	0.06	2.7	7.5	0.02	
1/29/85	U	24	0.37	0.21/0.52	66	6	−0.12	+0.23	0.08	2.7	23.6	0.04	
1/30/85	I	28	0.26	0.17/0.33	100	4	−0.11	−0.14	0.04	2.7	2.4	0.04	
1/30/85	V	18	0.29	0.19/0.38	91	5	−0.13	−0.07	0.05	2.7	11.1	0.03	
1/30/85	U	28	0.38	0.21/0.53	59	6	−0.05	+0.29	0.08	2.7	15.0	0.04	
1/31/85	I	26	0.52	0.44/0.60	105	2	−0.31	−0.31	0.04	2.7	2.7	0.05	
1/31/85	V	20	0.34	0.23/0.43	103	4	−0.14	−0.21	0.05	2.7	7.4	0.03	
1/31/85	U	32	0.41	0.28/0.55	74	5	−0.22	+0.17	0.07	2.7	35.3	0.03	
2/01/85	I	20	0.36	0.21/0.50	106	5	−0.17	−0.25	0.07	2.7	5.1	0.05	
2/02/85	I	14	0.33	0.10/0.55	109	9	−0.13	−0.27	0.11	2.7	1.3	0.18	†
2/04/85	I	24	0.20	0.07/0.32	93	8	−0.07	−0.08	0.06	2.7	0.4	0.08	†
2/05/85	I	20	0.18	0.00/0.33	98	11	−0.06	−0.11	0.08	2.7	0.3	0.13	†
2/06/85	I	30	0.51	0.38/0.62	105	3	−0.30	−0.30	0.06	2.7	6.0	0.06	
2/06/85	V	12	0.33	0.14/0.50	99	7	−0.16	−0.17	0.09	2.7	0.7	0.12	†
2/07/85	I	20	0.19	0.09/0.29	50	7	+0.10	+0.15	0.05	2.7	0.6	0.11	†
2/07/85	V	10	0.39	0.22/0.54	91	6	−0.23	−0.08	0.08	2.7	0.6	0.09	†
4/10/85	I	22	0.42	0.36/0.48	81	2	−0.26	+0.08	0.03	2.7	2.0	0.04	
4/10/85	V	16	0.47	0.33/0.61	71	4	−0.21	+0.23	0.07	2.7	2.5	0.02	
4/10/85	U	34	0.48	0.29/0.65	72	5	−0.26	+0.24	0.09	2.7	20.0	0.03	
4/11/85	I	20	0.51	0.38/0.62	80	3	−0.34	+0.12	0.06	2.7	14.4	0.02	
4/11/85	U	32	0.47	0.28/0.64	84	5	−0.34	+0.05	0.09	2.7	1.8	0.03	
4/13/85	I	24	0.28	0.22/0.34	78	3	−0.12	+0.06	0.03	2.7	3.6	0.04	
4/13/85	U	24	0.12	0.00/0.24	114	14	+0.04	−0.16	0.07	2.7	1.9	0.09	
4/14/85	I	32	0.00	0.00/0.00	...	...	+0.15	+0.01	0.08	2.7	0.4	0.30	†
4/14/85	V	32	0.17	0.07/0.27	53	8	+0.11	+0.11	0.05	2.7	4.6	0.05	
4/14/85	U	32	0.51	0.34/0.68	63	5	−0.17	+0.37	0.09	2.7	17.8	0.02	
4/15/85	I	40	0.11	0.00/0.24	4	15	+0.27	−0.03	0.07	2.7	1.0	0.08	
4/15/85	U	40	0.22	0.10/0.34	54	7	+0.06	+0.17	0.06	2.7	34.9	0.03	
4/16/85	I	20	0.46	0.33/0.57	36	4	+0.28	+0.38	0.06	2.7	3.0	0.03	
4/16/85	U	32	0.23	0.11/0.35	66	6	−0.03	+0.13	0.06	2.7	30.9	0.02	
5/31/86	I	24	0.40	0.29/0.49	78	3	−0.22	+0.11	0.05	2.7	4.1	0.05	
5/31/86	V	24	0.50	0.37/0.61	68	3	−0.20	+0.28	0.06	2.7	18.9	0.01	
5/31/86	U	24	0.49	0.33/0.65	66	5	−0.20	+0.32	0.08	2.7	15.2	0.02	
6/01/86	I	24	0.24	0.16/0.31	68	5	−0.04	+0.12	0.04	2.7	43.2	0.03	
6/01/86	V	24	0.24	0.09/0.38	74	8	−0.05	+0.07	0.07	2.7	10.5	0.02	
6/01/86	U	24	0.33	0.14/0.50	56	8	+0.01	+0.26	0.09	2.7	51.1	0.03	
6/02/86	I	24	0.27	0.16/0.36	67	5	−0.05	+0.15	0.05	2.7	2.4	0.03	
6/02/86	V	24	0.29	0.20/0.37	69	4	−0.06	+0.14	0.04	2.7	20.6	0.01	
6/02/86	U	24	0.34	0.15/0.51	64	7	−0.08	+0.22	0.09	2.7	23.1	0.03	
6/03/86	I	24	0.23	0.13/0.33	60	6	+0.02	+0.16	0.05	2.7	18.3	0.04	
6/03/86	V	24	0.38	0.25/0.49	67	4	−0.10	+0.21	0.06	2.7	42.6	0.01	
6/03/86	U	24	0.36	0.15/0.56	70	8	−0.15	+0.19	0.10	2.7	58.9	0.02	
6/04/86	I	24	0.31	0.20/0.40	53	5	+0.05	+0.25	0.05	2.7	13.0	0.05	
6/04/86	V	24	0.37	0.29/0.45	64	3	−0.06	+0.23	0.04	2.7	14.6	0.02	
6/04/86	U	24	0.27	0.07/0.44	71	9	−0.09	+0.13	0.09	2.7	97.6	0.02	

(1/2) $\tan^{-1}(U/Q)$. Columns (8)–(10) give the normalized Stokes parameters Q/I and U/I, and the associated error, $\sigma(Q/I) = \sigma(U/I)$. The Stokes parameters have the interstellar Q/I and U/I values subtracted, whereas the unbiased polarization and position angle do not. We used the Simmons and Stewart (1985) estimators to unbias the observed values of polarization. The confidence intervals are computed for the true polarization. Although the level of polarization is low, only 10 of the 112 measurements are consistent with zero polarization, at the 95% confidence level. Zero polarization appears most frequently in the I band, where the accuracy is highest but the intrinsic polarization is often lowest. Column (11) gives the aperture of the measurement in arcseconds. Columns (12) and (13) list two figures of merit, which are discussed below.

Since MINIPOL measures the polarization of the object and the sky background in successive integrations, we calculate the amount of uncertainty introduced by this procedure. In general, the effect is small because the sky is much fainter than the object. Column (12) presents the ratio of the object polarized flux to sky polarized flux, $C_1 = (pI)_{obj}/(pI)_{sky}$. In a 2."7 aperture, 3C 273 is much brighter than the surrounding sky, by about 4.5 mag at I, 5.5 mag at V, and 6.5 mag at U. However, in the presence of moonlight, the sky polarization can be much higher than the polarization of 3C 273, making the polarized fluxes comparable. Column (12) shows that in most cases, the polarized flux of 3C 273 completely dominates the polarized sky flux ($C_1 \gg 1$), and so the sky subtraction is unimportant. Column (13) has the ratio of the error in the polarized flux of the sky to the polarized flux of 3C 273, $C_2 = (\sigma_p I)_{sky}/(pI)_{obj}$. This number determines how accurately the sky polarization is measured. If C_2 exceeds the error of the individual Stokes parameter (col. [6]), then the measurement is affected by sky polarization. In most cases, C_2 equals a few hundredths, so the error in Q/I and U/I from 3C 273 is dominated by photon statistics. We use both of these indicators in a figure of merit for the polarization measurement. In Table 5, we arbitrarily choose $C_1/C_2 > 10$ as the criterion for a poor quality measurement, and flag these observations with a dagger. Twelve observations are affected; excluding them does not change the conclusions of this paper.

As a final check on the sky subtraction procedure, we plot the distribution of $\theta_{sky} - \theta_{obj}$ for objects of polarization $p < 3\%$, S/N > 1. In addition to 3C 273, a number of quasars, radio sources, and stars were measured for low-level wavelength-dependent polarization. Figure 4 shows the histogram of $\theta_{sky} - \theta_{obj}$ for 36 observations of 3C 273 and 153 observations of other low-polarization objects. Measurements in the I band are used, where the sky contamination is generally largest. Sky contamination would appear as a peak at low values of $\theta_{sky} - \theta_{obj}$, but the histogram in Figure 4 is statistically flat.

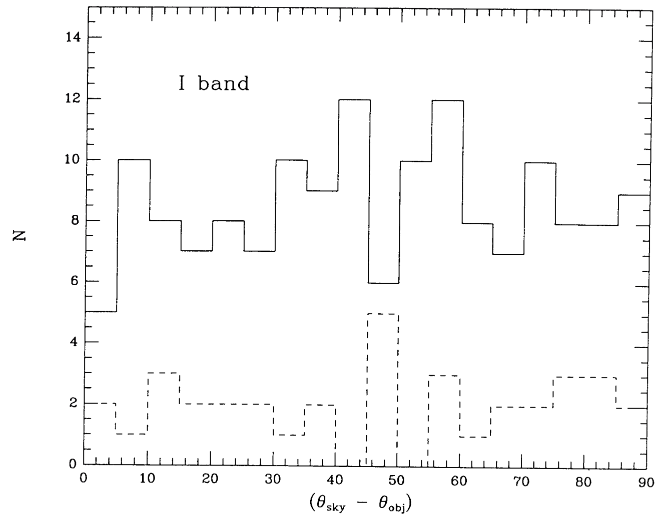

FIG. 4.—Histogram of differences between I-band polarization position angles of source and sky, in degrees. Includes observations of 3C 273 (*dashed line*) and other low-polarization objects (*solid line*). Measurements with sky contamination would show up as a peak at $\theta_{sky} \sim \theta_{obj}$.

The observed polarization of 3C 273 is comparable to the interstellar polarization in the solar neighborhood. To gauge the strength of the interstellar component, we made 15 white light polarization observations of seven stars within 0.°5 of the quasar; these stars are listed in Table 6. The UT date and star name are in columns (1) and (2). Stars labeled "A", "G", "D", and "B" are from Smith *et al.* (1985), and star 1 is the bright unpolarized standard HD 119447. Stars 2 and 3 have offsets from 3C 273 of $\Delta\alpha = 60$ W, $\Delta\delta = 65$ S, and $\Delta\alpha = 450$ W,

TABLE 6

3C 273 COMPARISON STARS

UT Date (1)	Star (2)	Time (minutes) (3)	Q/I (4)	U/I (5)	$\sigma(Q/I)$ (6)	Aperture (7)	C_1 (8)	C_2 (9)
1984 Mar 23	G	10	−0.05	+0.10	0.04	2."7	0.4	0.27[a]
1984 Mar 27	G	16	−0.17	+0.14	0.02	2.7	3.3	0.05
1984 Mar 27	D	8	−0.13	+0.06	0.03	2.7	4.4	0.03
1984 Mar 27	B	8	−0.04	+0.15	0.04	2.7	8.0	0.02
1985 Apr 10	G	8	−0.10	−0.04	0.04	2.7	0.2	0.12[a]
1985 Apr 10	D	8	−0.16	+0.07	0.02	2.7	0.7	0.04
1985 Apr 10	B	8	−0.14	+0.02	0.03	2.7	0.4	0.06
1985 Apr 14	G	8	−0.13	+0.14	0.07	2.7	1.9	0.06
1985 Apr 14	D	8	−0.25	+0.04	0.04	2.7	6.2	0.03
1985 Apr 14	A	8	−0.36	−0.39	0.20	2.7	1.4	0.14[a]
1985 Apr 15	1	4	−0.19	+0.02	0.01	2.7	95.0	0.01
1986 Jun 1	D	12	−0.12	+0.09	0.05	2.7	3.0	0.08
1986 Jun 1	2	8	−0.14	+0.10	0.02	2.7	8.6	0.02
1986 Jun 1	3	12	−0.11	+0.15	0.04	2.7	6.0	0.08
1986 Jun 4	2	12	−0.09	+0.09	0.03	2.7	4.5	0.04

[a] Observations with $C_1/C_2 < 10$.

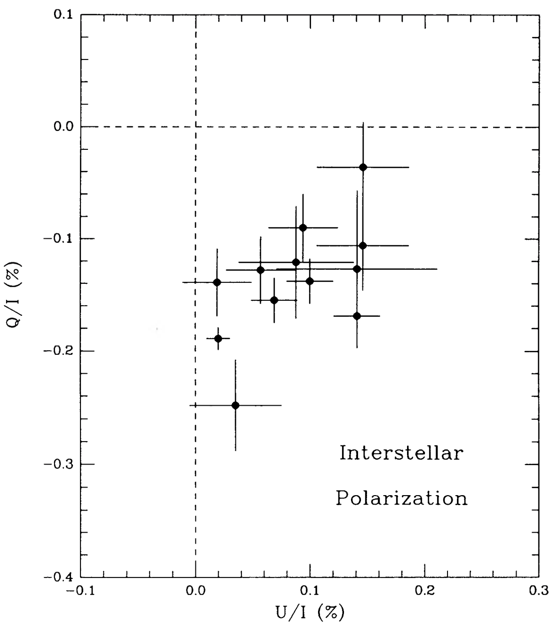

FIG. 5.—Normalized Stokes parameters Q/I and U/I (in percent) are plotted for 12 white light measurements of seven faint stars within 0°.5 of 3C 273. Average values define the interstellar polarization in the direction of the quasar.

$\Delta\delta = 155$ N arcsec, respectively. The integration time, normalized Stokes parameters, error, and aperture size are in columns (3)–(7). The quantities C_1 and C_2 are in columns (8) and (9); only observations with $C_1/C_2 < 10$ are used to calculate an average interstellar polarization. Six of the comparison stars lie in the magnitude range $11 < V < 13$, with colors $0.3 < U-V < 0.7$. Main-sequence stars and dwarfs with these values must be located well beyond the volume ($\sim 10^8$ pc^3) where the local magnetic field imprints interstellar polarization (Verschuur 1970). Small but significant interstellar polarization is observed in the direction of 3C 273; the weighted means of the Stokes parameters in percent are $Q/I = -0.161 \pm 0.072$ and $U/I = 0.061 \pm 0.088$. The data from Table 6 are plotted in Figure 5.

III. POLARIMETRIC PROPERTIES

The principal result of this paper is that 3C 273 has many of the polarization properties of blazars or BL Lac objects, although at a much lower level. The first week of observation in 1984 included a flare where the I-band polarization rose from 0.5% to 1.8% and fell back to below 0.5%. The polarization was larger at long wavelengths during the flare. The polarization position angle rotated with time, but not with wavelength. Figure 3 shows the degree of polarization in three wave bands, and the polarization position angle in the I band during the flare. Contemporaneous observations have been published by Smith *et al.* (1987). They record an R-band polarization of 0.6 ± 0.2% on 1984 March 21, before the flare event, and a value of 0.2 ± 0.1% on 1984 March 28, after the flare event. The latter result is within 2 σ of our measurement of 0.40 ± 0.06% on the same day.

During the remaining observations, the polarization was never greater than 1% in any wave band. Recently, Courvoisier *et al.* (1988) have measured a polarization flare with a peak amplitude of 2.5%. Episodes of high polarization are rare in this quasar. Previous high-quality observations have not found polarization above 1% at optical or infrared wavelengths (Whiteoak 1966; Liller 1969; Kemp *et al.* 1977; Knacke, Capps and Johns 1979; Stockman, Moore, and Angel 1984; Smith *et al.* 1987). Out of 73 observations of 3C 273 since 1963, seven are above 1%, and only two exceed 2%. However, real polarization variations were observed throughout our 28 months of observation. Most published polarization measures for AGNs have errors of 0.3%–1.0%. The rich and complex polarization behavior of 3C 273 is clearly revealed by more accurate polarimetry.

To derive the intrinsic polarization of 3C 273, interstellar polarization has been subtracted from the Stokes parameters in Table 5. The stars near 3C 273 were observed unfiltered for high accuracy, but interstellar polarization has a wavelength dependence. Serkowski, Mathewson, and Ford (1975) have shown that nearby stars with high galactic latitude ($b^{\rm II} = 63°$ for 3C 273) and very low $p_{\max}$ ($\ll 1$%) have small amounts of color excess and reddening, $E_{B-V} < 0.10$. The reddening for 3C 273 is $E_{B-V} = 0.05$ (Wu 1977). The stars in Table 6 have a mean $B-V = 0.57$, so we convolve the appropriate main-sequence energy distribution with the instrument response to get the effective wavelength for the white light polarization data, $\lambda_{\rm eff} = 5330 \pm 10$ Å. Since $\lambda_{\max} = 0.555\lambda - 0.03E_{B-V}$, take $\lambda_{\max} \sim 5500$ Å. An interstellar polarization is calculated for each filter, using the Serkowski (1974) relation $p(\lambda)/p_{\max} = \exp[-1.15 \ln^2(\lambda_{\max}/\lambda)]$. The adopted Stokes parameters for interstellar polarization are listed in Table 7.

Our discussion of variability uses normalized Stokes parameters. The addition and subtraction of multiple components is linear, as long as the intensity is constant, which is confirmed at the 10% level by our photometry. Figure 6 shows all measurements of Q/I and U/I in percent for 3C 273, after interstellar polarization has been subtracted. Different observing runs have different symbols. Data points from the two peak nights of the 1984 March flare are outlined with circles. The interstellar correction is shown as a vector on the figure. Additional figures are used to display Q/I and U/I as a function of both time and wavelength. Figures 7*a*, 7*b*, and 7*c* show the data for all observing runs separated by filter, with individual error bars. From these figures, we deduce that the polarization variability increases toward longer wavelengths, and that the polarization never completely disappears.

Average Stokes parameters and internal errors for each observing run are listed in Table 8. Column (1) lists the observing run, and columns (2) and (3) give the number of observations and the filter. Normalized Stokes parameters Q/I and U/I and the error in both are contained in columns (4)–(6), with the unbiased polarization, 95% confidence interval, position angle, and position angle error [$\sigma(\theta) = 27.6\ \sigma(p)/p$ degrees] listed in columns (7)–(10). In addition to the high-precision filtered measurements, we searched for rapid-

TABLE 7

INTERSTELLAR POLARIZATION FOR 3C 273

Filter (1)	$p/p_{\max}$ (2)	Q/I (3)	U/I (4)
U	0.81	−0.130	0.049
B	0.96	−0.155	0.059
V	1.00	−0.161	0.061
R	0.94	−0.151	0.057
I	0.85	−0.137	0.052

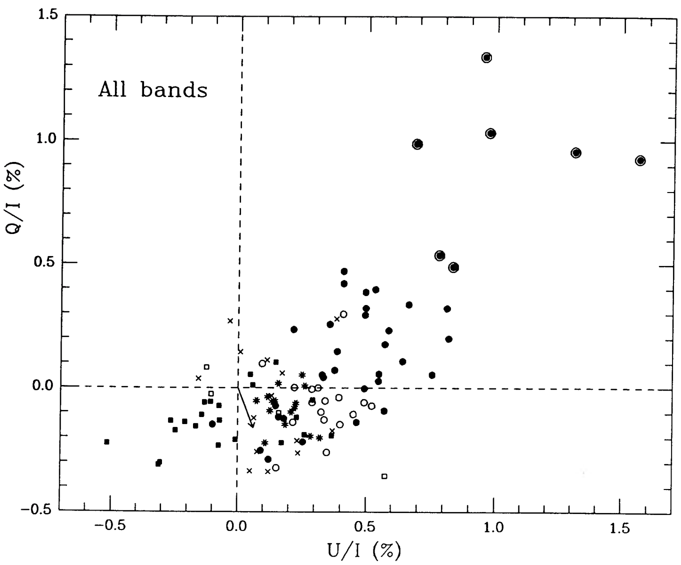

FIG. 6.—Normalized Stokes parameters (in percent) for 3C 273, with different symbols for observing runs A (*filled circles*), B (*open circles*), C (*open squares*), D (*filled squares*), E (*crosses*), and F (*asterisks*). The 1984 March flare is outlined with circles. Interstellar polarization has been subtracted and is shown as a vector.

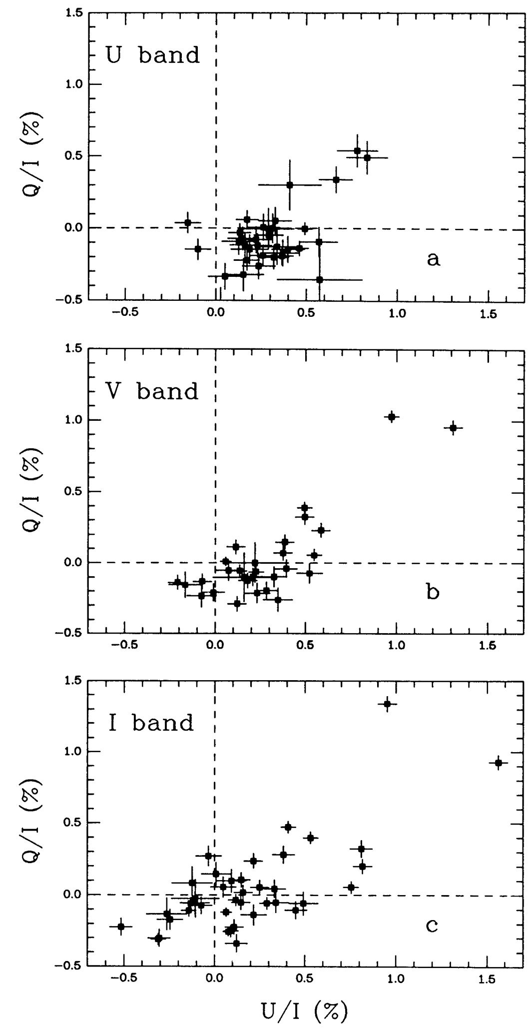

FIG. 7.—Same as Fig. 6, but data have individual error bars added and are separated by wavelength into (*a*) *U*-band, (*b*) *V*-band, and (*c*) *I*-band measurements.

polarization variability on 1985 January 29, at a time when the polarization state was low, with a series of unfiltered, 1 minute integrations. Figure 8 shows the variations, and a χ^2 test gives only a 70% confidence level that real variations are detected. This leads to an upper limit on rapid variability.

The polarization properties of 3C 273 can be summarized as follows:

1. The *I*-band polarization is highly variable, with changes on all time scales from days to years. Position angle rotations of up to 90° are observed. The amplitude of the polarization is low, with a peak of under 2%. Polarization changes trace out a random walk on the Q/I versus U/I plane.

2. The maximum observed change in polarization is 1.0% in 24 hr. A search for rapid variability gives a 3 σ limit of 0.2%

TABLE 8

POLARIZATION AVERAGES

Run (1)	Observations (2)	Filter (3)	Q/I (4)	U/I (5)	$\sigma(Q/I)$ (6)	p (7)	$\sigma(p)$ (95% confidence) (8)	θ (9)	$\sigma(\theta)$ (10)
A	10	*I*	+0.34	+0.61	0.02	0.70%	0.66/0.75	30°	1°
	10	*V*	+0.31	+0.57	0.02	0.65	0.61/0.69	31	1
	10	*U*	+0.00	+0.41	0.02	0.40	0.34/0.47	45	1
B	6	*I*	−0.06	+0.32	0.03	0.32	0.27/0.37	50	3
	5	*V*	−0.10	+0.39	0.03	0.40	0.33/0.47	52	2
	6	*U*	−0.09	+0.32	0.05	0.33	0.23/0.42	53	4
C	2	*I*	+0.03	−0.12	0.08	0.09	0.00/0.24	...	...
	2	*V*	−0.10	+0.16	0.17	0.08	0.00/0.35	...	...
	2	*U*	−0.51	+0.24	0.14	0.54	0.25/0.81	77	7
D	11	*I*	−0.13	−0.17	0.02	0.21	0.18/0.24	116	3
	6	*V*	−0.09	−0.03	0.02	0.09	0.05/0.13	99	6
	5	*U*	−0.16	+0.27	0.03	0.32	0.25/0.38	60	3
E	6	*I*	−0.12	+0.09	0.02	0.15	0.11/0.19	72	4
	2	*V*	+0.00	+0.15	0.04	0.15	0.06/0.23	45	7
	6	*U*	−0.07	+0.03	0.03	0.13	0.07/0.19	78	6
F	5	*I*	−0.05	+0.15	0.02	0.16	0.12/0.20	54	3
	5	*V*	−0.08	+0.19	0.02	0.21	0.16/0.25	56	3
	5	*U*	−0.11	+0.23	0.04	0.25	0.17/0.33	58	4

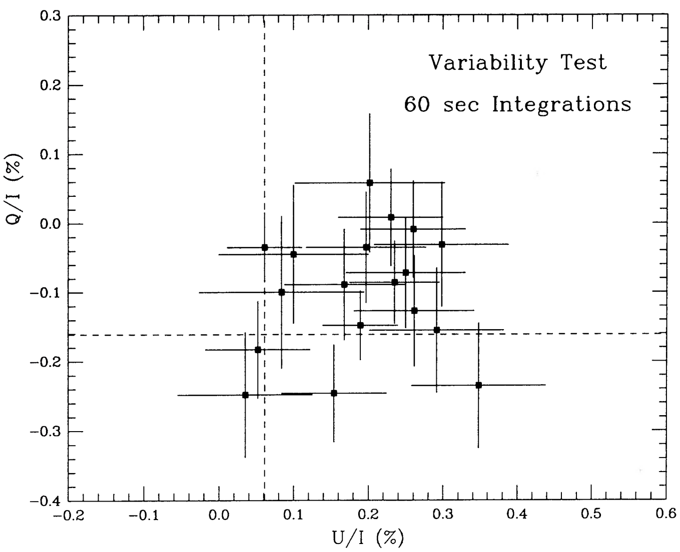

FIG. 8.—Normalized Stokes parameters for a series of 1 minute unfiltered observations of 3C 273. No rapid variability was detected.

in 20 minutes. At the peak of the flare, when the polarization changed by 1%, the total flux density changed by less than 10% (2 σ), implying that the intrinsic polarization of the variable component is greater than 10%.

3. When the polarization is strongest, the degree of polarization increases toward longer wavelengths. Wavelength dependence of the position angle is generally absent. Conversely, when the polarization is weakest and no variability is seen, the degree of polarization increases toward shorter wavelengths.

4. The ultraviolet polarization is quiescent and nonzero. A careful determination of the interstellar polarization in the direction of 3C 273 demonstrates that this low-level polarization is intrinsic to the quasar. Excluding data taken during the 1984 March flare, the U-band observations are consistent with a fixed polarization at a level of 0.3% and a position angle of $60° \pm 10°$.

IV. THE NATURE OF THE POLARIZATION

The behavior of linear polarization in 3C 273 is complex. It is unlikely that a single component or emission mechanism can account for the results. Moreover, it has been known for some time that the optical energy distribution of 3C 273 comprises at least two components (Malkan and Sargent 1982). A comprehensive model for the emission must incorporate the Stokes parameters Q, U, and I. The three characteristics of the polarization that can be used to constrain emission models are variability, amplitude, and wavelength dependence.

a) Polarization Variability

The variability can be used to rule out polarization by scattering from large dust grains. Edelson and Malkan (1986) have argued that dust is not a strong component in most quasars and blue Seyfert 1 nuclei. There is little or no reddening of the recombination lines in 3C 273, and the 3.3 μm dust feature is not present (Lee *et al.* 1982). Although 3C 273 has a possibly thermal excess at ~ 5 μm, it is a small component of the total luminosity. Dust emitting at shorter wavelengths would have a temperature of ~ 2000 K and could not survive close to the AGNs. The minimum size of the thermally emitting region is $T_d^2 (L_d/4\pi\sigma)^{1/2} = 2 \times 10^{21}$ cm, where T_d is the dust temperature and L_d is the infrared luminosity. If polarization is imprinted in the same volume as the overall optical continuum, then the variability indicates a source size of $\sim 3 \times 10^{15}$ cm.

Owing to its variable polarization, 3C 273 differs from other AGNs that have low levels of polarization. Antonucci (1984) and Rudy *et al.* (1983) found that polarization changes in radio galaxies and Seyferts do not usually involve large rotations in position angle. These authors find an upper bound to the variability of $\Delta p/p \leq 1$ and $\Delta\theta \leq 10°$. Quasars with low-level polarization do not vary, with 90% confidence limits of $\Delta p/p \leq 0.16$ and $\Delta\theta \leq 8°$ on a time scale of 1 yr (Stockman, Moore, and Angel 1984). The steady position angle in most quasars is important, because it means that the low-level polarization is probably not a diluted version of the blazar phenomenon. By contrast, 3C 273 displays polarization changes of $\Delta p/p \gg 1$ and $\Delta\theta > 90°$. It is possible that 3C 273 lacks the constant polarization component that is present in many other radio sources.

b) Degree of Polarization

The polarization variations in 3C 273 are strikingly similar to the variations in BL Lac objects or blazars. However, in most blazars, the median optical polarization is 10%–15%, and it can be as high as 45% (Angel and Stockman 1980). The median optical polarization of 3C 273 is below 0.5%. We point out that the variable polarization in 3C 273 is the first direct indication of synchrotron emission at optical wavelengths. It is necessary to explain why the level of polarization is so low. Scattering by small particles is ruled out by the variability. Faraday depolarization can be caused by a thermal electron plasma with an embedded magnetic field. The Faraday rotation of position angle is $\phi \sim 2 \times 10^{-4} \nu^{-2} n_e B \cos\theta$ rad cm^{-1}, where n_e is the electron number density, B is the magnetic field, and θ is the angle between B and the line of sight. Modest field strengths are sufficient to make the integral of ϕ over the path length much greater than 1 rad, destroying the polarization. However, the rapid variability is difficult to explain if the Faraday optical depth is high.

Low degrees of synchrotron polarization can also be produced by a stochastic model, where a number of highly polarized subunits are switching on and off (Blandford and Rees 1978). A composite source will show random walk variations in the Q/I–U/I plane. This behavior has been observed in a number of blazars at optical (Moore *et al.* 1982; Brindle *et al.* 1986; Sitko, Schmidt, and Stein 1985) and radio wavelengths (Jones *et al.* 1985). The I-band variations of 3C 273 shown in Figure 7*c* trace a stochastic path in Q/I and U/I. But if the multiple components have randomly oriented magnetic fields, the model fails to account for the data. With n_c individual components of synchrotron polarization p_c, the polarization of the ensemble is $p_c n_c^{-1/2}$. The typical changes in total intensity, polarization, and position angle are n_c^{-1}, p_c/n_c%, and $n_c^{-1/2}$ rad, respectively. Although Moore *et al.* (1982) matched the variations of BL Lac with $p_c \sim 70\%$ and $n_c \sim 10$, 3C 273 has both a low degree of polarization *and* large swings in position angle. If $p_c \sim 10\%$, about 200–300 subunits give the correct degree and variability of polarization, but allow only small position angle swings of under 5°. If n_c is small, then p_c must be low, and the individual components no longer have blazar properties.

Optical monitoring has shown that blazars with maximum polarizations above 15% are rarely observed with $p < 1\%$

(Angel *et al.* 1978). Therefore, we favor the explanation that 3C 273 has intrinsically high polarization ($\Delta B^2/B^2 = 0.1$–0.2) which is diluted by an unpolarized component, rather than synchrotron emission with an isotropic magnetic field and intrinsically low polarization ($\Delta B^2/B^2 \sim 0.005$). In the synchrotron interpretation, $\Delta B^2/B^2$ is a measure of the isotropy of the magnetic field, $\Delta B^2/B^2 = |\langle B_\perp^2 \rangle - \langle B_\parallel^2 \rangle|/|\langle B_\perp^2 \rangle + \langle B_\parallel^2 \rangle|$. The low degree of variable polarization is explained by a blazar synchrotron source which is diluted by a normal low-polarization quasar component. We propose that the optical flux density consists of $\sim 90\%$ low-polarization component and $\sim 10\%$ miniblazar.

c) *Wavelength Dependence of Polarization*

Figure 7 shows that the polarization variations increase toward longer wavelengths. The amplitude of polarization is largest in the *I* band, but it does not become zero in the *U* band. Malkan and Sargent (1982) have decomposed the continuum of 3C 273 into a power law, and a thermal component which dominates at short wavelengths. Our simple model for the data assumes that the thermal spectrum is unpolarized with flux density $S_{bb}(\lambda)$, and that the power law has a flux density $S_{pl}(\lambda)$ and a polarization *p*, which is independent of wavelength. The resultant polarization from the two components is $p[1 + S_{bb}(\lambda)/S_{pl}(\lambda)]^{-1}$. The continuum model gives ratios $S_{bb}(\lambda)/S_{pl}(\lambda)$ of 3.02 (*U*), 2.27 (*B*), 1.74 (*V*), 1.15 (*R*), and 0.95 (*I*). The thermal component increasingly dilutes the power-law polarization toward shorter wavelengths, so that the net polarizations of the power-law component are $0.25p$ (*U*), $0.31p$ (*B*), $0.37p$ (*V*), $0.47p$ (*R*), and $0.51p$ (*I*).

This simple decomposition can account for the wavelength dependence of polarization during the 1984 March flare. The model predicts polarization ratios of $p(I)/p(V) = 1.38$ and $p(I)/p(U) = 2.04$. The average polarization ratios from March 23 to 27 are $p(I)/p(V) = 1.29 \pm 0.15$ and $p(I)/p(U) = 1.76 \pm 0.33$. There are other constraints. First, the thermal spectrum only dilutes the polarization by a factor of 2 in the *I* band and a factor of 4 in the *U* band. This implies a power-law polarization with a peak of under 4% and a typical level of $\sim 1\%$, well below typical blazar levels. In other words, dilution by a thermal component *alone* does not explain the polarization being so far below typical blazar levels. Second, the polarization varied by $\sim 1\%$ across the peak of the flare, but the photometry shows that the flux density changed by less than 10% ($2\ \sigma$). Therefore, the variable flux component *must* have an intrinsic polarization 10% or greater. We therefore propose two spectral components in 3C 273: $\sim 90\%$ of the optical flux density from a typical quasar, consisting of a low-polarization power law and a thermal spectrum that rises toward ultraviolet wavelengths; plus $\sim 10\%$ of the optical flux density from the polarized power law of a typical blazar.

d) *Quiescent Polarization*

In addition to the variable *I*-band polarization, there is a small but persistent level of polarization in the *U* band (it is also apparent in the polarimetry reported by Courvoisier *et al.* 1988, despite their larger uncertainties). If observations from the flare event in 1984 March are excluded, the scatter in Figure 7*a* is consistent with a fixed value of *Q*/*I* and *U*/*I*. The degree of polarization of this quiescent component is only 0.3%, so we must be confident of the correction for interstellar polarization. The level of interstellar polarization is low, and so the position angle is poorly determined in Figure 5. However, the mean observed *U*-band Stokes parameters for 3C 273 (excluding 1984 March) are $Q/I = -0.27$ and $U/I = 0.32$. That level of interstellar polarization is ruled out at the 99% confidence level. Alternatively, our adopted relation for $p(\lambda)/p_{max}$ may be inappropriate. However, it would take a value of λ_{max} well outside the range observed by Serkowski, Mathewson, and Ford (1975) to double the calculated *U*-band interstellar polarization. If the field stars are representative of interstellar polarization in the direction of 3C 273, then the quiescent *U*-band polarization must be intrinsic to the quasar.

We can estimate the wavelength dependence of the quiescent polarization component using the data from 1986 May–June. Constant polarization is seen at all three wavelengths in Table 8. We assume that the miniblazar component was at a low level, and that the polarization comes from the quiescent component. The assumption is justified by the fact that the averages for 1986 May–June (run F in Table 8) show polarization increasing toward *shorter* wavelengths. The polarization ratios are $p(I)/p(V) = 0.80 \pm 0.53$ and $p(I)/p(U) = 0.65 \pm 0.44$. This wavelength dependence is inconsistent with the model used in the last section to explain the flare polarization, at a 99% confidence level. Consider instead a model with a thermal spectrum of flux density $S_{bb}(\lambda)$ and polarization *p*, and an unpolarized power law of flux density $S_{pl}(\lambda)$. The power law dilutes the thermal component polarization toward longer wavelengths, so that the net polarizations become $0.75p$ (*U*), $0.69p$ (*B*), $0.63p$ (*V*), $0.53p$ (*R*), and $0.49p$ (*I*). The polarization ratios of the new model are $p(I)/p(V) = 0.78$ and $p(I)/p(U) = 0.65$, in excellent agreement with the data.

The quiescent polarization may be due to scattering; a nearly spherical scattering geometry with optical depth in the range $0.1 < \tau < 50$ can readily produce $\leq 1\%$ polarization. The model assumed wavelength-independent polarization for the thermal component. Scattering by small dust grains rises into the blue as $p \propto \lambda^{-4}$; this wavelength dependence is ruled out by the data at the 98% confidence level. Electron scattering at optical wavelengths ($h\nu \ll m_e c^2$) is independent of wavelength, consistent with the model. Courvoisier *et al.* (1987) have found little or no intrinsic absorption of the X-ray source. Ulrich, Courvoisier, and Wamsteker (1988) contend that the variable UV flux in 3C 273 may be the result of a rapidly variable inner source surrounded by an optically thick medium. The optically thick medium will thermalize the original source spectrum and smooth out time variations, but it will also destroy linear polarization efficiently. They derive a photon mean free path of $\sim 4 \times 10^{13}$ cm and about 10^4 scatterings. This optical depth would reduce polarization to undetectable levels, unless the surrounding medium is asymmetric. There are many places between the solar neighborhood and the core of 3C 273 where such a small amount of quiescent polarization could be imprinted. In what follows, we assume that it comes from the thermal ultraviolet emission of an accretion disk.

Since the "blue bump" component accounts for an increasing fraction of the continuum at shorter wavelengths, Webb and Malkan (1986) proposed that the polarization in LPQs is entirely attributable to a uniformly polarized blue bump. The decomposition of the 3C 273 spectrum is consistent with this suggestion. The "blue bump" in 3C 273 is well described by an optically thick, geometrically thin accretion disk around a black hole of $5 \times 10^8\ M_\odot$ (Malkan 1983). The blue bump is expected to have some intrinsic polarization because the opacity in the disk atmosphere is dominated by electron scattering. Unless the disk is viewed face-on, its thermal emission will emerge with some net polarization. The electric field vector will be either parallel or perpendicular to the disk rotation axis, depending on the electron scattering optical depth (Webb and Malkan 1986) and the degree of irregularity of the disk surface (Coleman and Shields 1990). Simple disk and jet models predict that the position angle of the jet should be identical to that of the disk rotation axis (i.e., the jet emerges along the disk poles). Thus, the disk polarization position angle would be expected to be parallel or perpendicular to the VLBI position angle of 43°. The quiescent polarization position angle is 60° ± 10°, which is marginally inconsistent with the simple model.

The interpretation of the 3C 273 polarization leads to the following conclusions:

1. The variable polarization cannot be explained by a dust model; the synchrotron process is the most likely emission mechanism. In contrast to 3C 273, most AGNs with low polarization do not show large fractional changes in p and θ. However, few AGNs have polarimetry of sufficient accuracy to reveal variable polarization at the level that is found in 3C 273.

2. The polarized component in 3C 273 has all the characteristics of a blazar, except that the amplitude of the polarization is an order of magnitude too low. It is unlikely that the low polarization is caused by many highly polarized but randomly oriented subunits, or by Faraday depolarization.

3. Changes in polarization and flux density during the 1984 March flare show that a small fraction of the total flux varies, and that the polarization of the variable component is at least 10%.

4. We favor a model where ~10% of the optical flux comes from a highly polarized blazar power law, and ~90% comes from a typical low-polarization quasar component (i.e., optical/infrared power law plus ultraviolet thermal spectrum). If the ultraviolet thermal component is unpolarized or has very low polarization, then a deconvolution yields wavelength-independent polarization for the power law.

5. The detection of a miniblazar in 3C 273 strengthens the link between superluminal motion at radio wavelengths and blazar activity at optical wavelengths. At maximum polarization, the position angle represents a magnetic field perpendicular to the jet axis.

6. The origin of the quiescent ultraviolet polarization is uncertain, but may arise from an accretion disk close to the power source. If the quiescent polarization comes from the thermal component of the spectrum, then the intrinsic polarization is 0.3%, and scattering by small dust grains is ruled out.

V. AN OVERVIEW OF 3C 273

The powerful technique of polarimetry has been used to study blazar activity in 3C 273. Two types of polarization behavior have been isolated. The variable polarization mimics the synchrotron characteristics of blazars, but at a reduced polarization level. The quiescent polarization is similar to the low polarization of most quasars. In this section, we relate the polarimetry to other observations of 3C 273 and discuss the connection between 3C 273 and other strong radio sources.

a) VLBI and Optical Properties

The core of 3C 273 has been monitored with VLBI at 5.0 and 10.7 GHz since 1977 (Unwin *et al.* 1985). Four components show apparent superluminal motion, with velocities $5.1 < v_{\rm app}/c < 8.0$ ($H_0 = 100$ km s^{-1} Mpc^{-1}, $q_0 = 0.5$). The knots

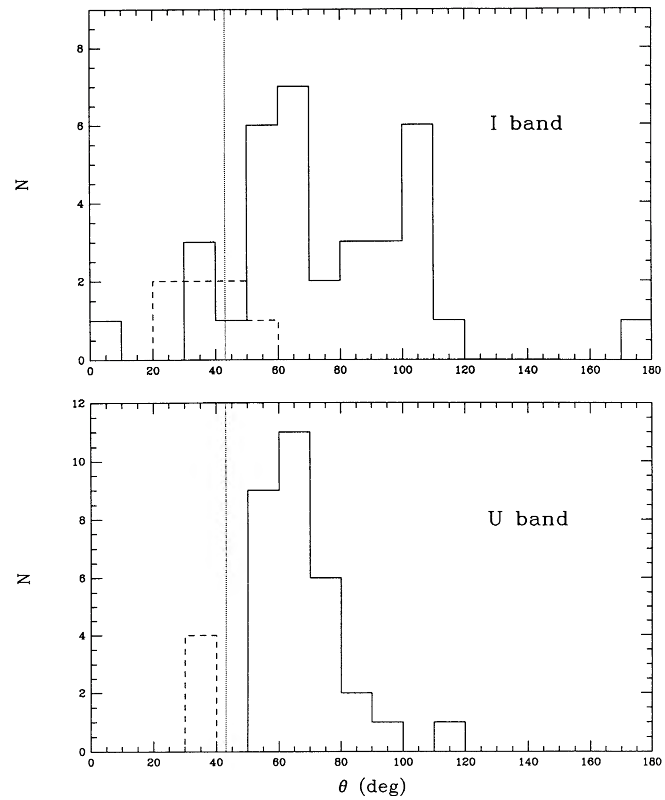

FIG. 9.—Distribution of polarization position angles in the (*a*) *I* and (*b*) *U* bands for all observations of 3C 273, including data from Courvoisier *et al.* (1988). Observations from the polarization flare of 1984 March 22–29 are plotted as a dashed histogram. The VLBI structure axis is drawn as a dotted line at 43°.

decay with half-lives of 2–3 yr as they move from the core along the jet. The inner jet shows many kinks and wiggles, but the position angle of the smallest structure (~1 pc, $\theta = 40°$–$50°$) agrees well with the position angle of the large outer jet (~100 kpc, $\theta = 43°$). Note that there is a π ambiguity in the definition of polarization position angle. The radio jet is continuous from the core to beyond the distance of the optical jet, with no evidence for a counterjet (Davis, Muxlow, and Conway 1985).

Polarization position angle is aligned with VLBI structure axis in blazars (Rusk and Seaquist 1985; Impey 1987). Figures 9*a* and 9*b* show the distribution of position angles for the data in Table 5 and of Courvoisier *et al.* (1988) in the *I* and *U* bands. Our measurements during the flare of 1984 March are shown as a dashed histogram. Alignment of the optical polarization with the radio jet axis occurred only during the polarization flare. The *I*-band polarization and position angle during the flare are plotted in Figures 2*c* and 2*d*. A clear and systematic position angle rotation by 30° is seen during the flare. Smooth position angle rotations were not observed at any other time during our observations. If the flare polarization is imprinted by optically thin synchrotron emission, then the magnetic field should be perpendicular to the radio jet axis. However, Röser and Meisenheimer (1986) find that the position angle of optical polarization in the extended jet is 139° ± 10°, corresponding to a magnetic field parallel to the radio jet axis.

It is tempting to associate the polarized optical flux with the radio emission on VLBI scales, but there is no evidence that the two emission sources are cospatial. The most direct comparison is with VLBI polarimetry. Published maps are rare, but show ejected knots with high polarization (5%–30%) and cores which are often unpolarized (Roberts and Wardle 1987). The only other galaxy with a large-scale polarized optical jet is M87. The four brightest condensations in the M87 jet have position angles of 127°, 128°, 124°, and 119°, while the core has an angle of 42° ± 8° (Warren-Smith, King, and Scarrott 1984). We do not know if a position angle rotation of 90° between core and jet polarizations is a characteristic feature of AGNs.

b) Energy Distribution and Variability

The variability of 3C 273 has been studied from 10^8 to 10^{18} Hz, revealing a complex pattern of variability. Flux variations of a factor of 2 or more on a time scale of several months have been observed at radio (Aller *et al.* 1985), millimeter, infrared (Robson *et al.* 1986; Cutri *et al.* 1985), optical (Sadun 1985; Courvoisier *et al.* 1987), ultraviolet (Courvoisier and Ulrich 1985), and X-ray wavelengths (Courviosier *et al.* 1987). Recently, Courvoisier *et al.* (1988) reported infrared variations of a factor of 2 on time scales as short as 1 day. Our interpretation of the data is that variability at all wavelengths comes from one nonthermal component. This component is responsible for the diluted polarization seen at optical wavelengths. We cannot rule out an additional variable component which is unpolarized. However, rapid variability, such as that shown by 3C 273, is almost always associated with polarized blazar emission (Stockman, Moore, and Angel 1984).

The duty cycle of large-amplitude flares in 3C 273 is long. Neugebauer *et al.* (1979) found few dramatic flux outbursts at optical and infrared wavelengths over a period of 12 yr. Far-infrared *IRAS* measurements by Edelson and Malkan (1987) find no evidence for far-infrared variability at the 10% level. Similarly, we have concluded that the duty cycle of polarization states where $p > 1\%$ is also long. Robson *et al.* (1986) found that variations can occur in phase from near-infrared to millimeter wavelengths. The amplitude of the variability increases with wavelength, from 10% or less at 0.55 μm, to 20% at 2.2 μm, 50% at 10 μm and a factor of 2 or 3 at 1 mm.

In Figure 10, the overall energy distribution of 3C 273 is plotted from radio to ultraviolet wavelengths. The variable "flare" spectrum was calculated by subtracting the quiescent flux level of 1986 February from the high-state fluxes of 1984 March–April (Curvoisier *et al.* 1987). The flare spectrum steepens from $\alpha \sim 0.8$ (10–1500 μm) to $\alpha \sim 1.5$ (1–4 μm), and the optical *V*-band point is the upper limit of 10% from the data in this paper. The thermal component dominates the energy distribution from 10^{14} to 10^{16} Hz. Figure 10 also includes the mean energy distribution of a large sample of blazars from Impey and Neugebauer (1988), scaled with arbitrary zero point. The "flare" spectrum is similar to this average blazar spectrum. Therefore, the miniblazar dominates at millimeter wavelengths ($p \leq 5.8\%$; Rudnick *et al.* 1985) and is diluted by a typical LPQ spectrum to a polarization of under 1% at optical wavelengths. The crosses represent the polarized flux density (pS_ν) at the peak of the polarization flare (1984 March 24). As a fraction of *total* flux density, the polarized flux is only ~1%. However, as a fraction of *power-law* flux density, the polarized flux is ~10%, the typical polarization of a blazar.

c) Beaming and Miniblazars

We have interpreted the 3C 273 spectrum as a mixture of low-polarization quasar and blazar components. Orr and

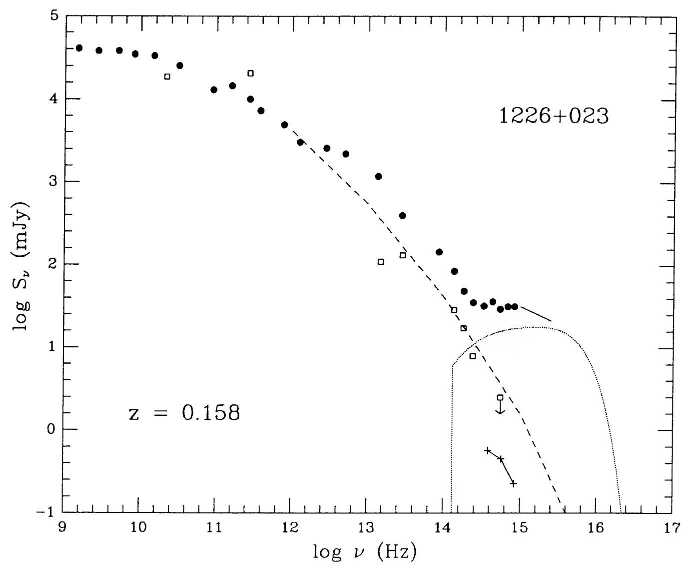

FIG. 10.—Energy distribution of 3C 273 from radio to ultraviolet wavelengths. Filled circles are mean total flux density; open squares represent the "flare" spectrum as described in the text. Dotted line is the ultraviolet thermal component, and dashed line is the mean blazar SED from Impey and Neugebauer (1988). Crosses show the polarized flux spectrum on 1984 March 24, at the peak of the polarization flare.

Browne (1982) have proposed a "unified" model of AGNs, with a combination of beamed and unbeamed components for the optical emission (Browne and Murphy 1987). At radio wavelengths, the compact emission (L_c) is beamed with Lorentz factor γ, and the extended emission (L_e) is isotropic. The observed ratio

$$R = \tfrac{1}{2}R_T[(1 - \beta \cos \theta)^{-(2-\alpha)} + (1 + \beta \text{ os } \theta)^{-(2-\alpha)}]$$

depends on the angle to the line of sight θ, the Lorentz factor, and R_T, which is the ratio L_c/L_e when $\theta = 90°$. The beamed component of the emission has two limiting values. Quasars with $R - R_T \ll R_T$ (i.e., steep radio spectrum), $L(\theta) \sim L_T$ have mostly unbeamed emission. Quasars with $R \gg R_T$ (i.e., flat radio spectrum), $L(\theta) \sim \frac{1}{2}(2R/R_T)^{1.35}$ have mostly beamed emission. At optical wavelengths, the transition between these cases depends on the amount of unbeamed emission. Murphy and Browne determined this amount by fitting ratios of optical to extended radio luminosity. The model for 3C 273 requires a quasar with $R \sim 6$ and $L_e = 5 \times 10^{26}$ W Hz^{-1}, with a predicted ratio of unbeamed to beamed optical emission of about 5. This ratio will dilute a typical blazar polarization of 10%–15% down to under 3%.

We can relate 3C 273 to other quasars with strong radio emission. Figure 11 shows the fraction of quasars in a complete radio sample (sources stronger than 2 Jy at 5 GHz) which have optical polarization above 3%. This is plotted as a function of radio compactness, i.e., the fraction of total radio flux density in an unresolved milliarcsecond core (Impey and Tapia 1990). The fraction of blazars increases strongly with radio compactness. Essentially, every radio source that is unresolved with VLBI techniques shows high polarization. The compactness parameter of 3C 273 is log ($S_{\text{mas}}/S_{\text{tot}}$) = −1.42. Since 3C 273 has a lower redshift than most 2 Jy quasars, the VLBI experiment probes a smaller physical size. Even when this is taken into account, the compactness of 3C 273 is below the median for radio quasars. Figure 11 shows that *most* quasars

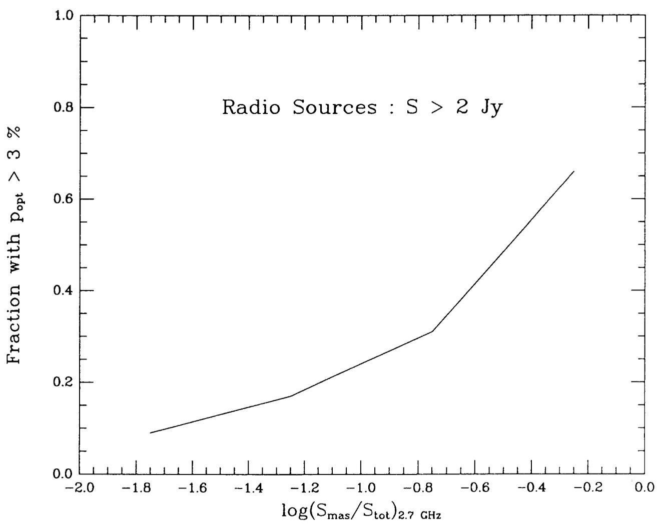

FIG. 11.—Fraction of quasars with optical polarization above 3% is plotted as a function of the fraction of 2.7 GHz flux density in an unresolved VLBI core. A complete sample of quasars stronger than 2 Jy at 5 GHz is used.

with the compactness of 3C 273 have *low* polarization. So the weakness of the 3C 273 polarization is not surprising. A more important issue is whether or not there is any fundamental difference between the quasars with high and low polarization. The detection of blazar activity in 3C 273 suggests that variable polarization can be found in other core-dominated quasars, but that it might be diluted down to a low level.

In models of bulk relativistic motion, beamed radiation will only dominate isotropic radiation for the small fraction of sources with large γ and small θ. To test this model, it is important to look for low-level polarization in the most core-dominated quasars, where the beamed component should be strongest. One approach is to survey quasars with R $(=L_c/L_e) > 1$ and low L_e. An alternative is to scrutinize the few superluminal radio sources with $p_{\rm opt} < 3\%$ for low-level variable polarization. Of course, the optical counterparts must be bright enough for polarimetry of the required precision.

An outline for the overall spectral properties of quasars may be as follows. All quasars, including the vast majority of optically selected QSOs, have a power law that turns over at far-infrared or millimeter wavelengths. This power law is quiescent, has low polarization, and may or may not be due to synchrotron emission. A thermal ultraviolet component is also present. Weak radio emission is seem, which is uncorrelated with the optical and infrared power law. Relativistic beaming is only associated with compact radio emission. When beaming is strong, a smooth synchrotron spectrum is seen from millimeter to ultraviolet wavelengths, and the emission is variable and polarized. When the beaming is weak, the synchrotron spectrum only dominates at millimeter and infrared wavelengths, and the optical polarization is low.

We gratefully acknowledge the expert assistance of Angel Guerra and Fernando Peralta at the Du Pont 100 inch (2.5 m) telescope and Oscar Duhalde at the 40 inch (1 m) telescope. Successful operation of MINIPOL was due in part to the excellent technical support of Las Campanas Observatory. Comments by the referee improved the presentation of this paper. C. D. I. thanks Caltech for a Weingart Fellowship and NOAO for travel support, and acknowledges support from NSF grant AST-8700741 and NASA/JPL contract 958028. M. A. M. acknowledges support from NSF grant AST-8614510. S. T. was supported in part by NASA grant INT 82-13103 and grant CW 0006-85 from the Space Telescope Science Institute.

REFERENCES

Aller, H. D., Aller, M. F., Latimer, G. E., and Hodge, P. E. 1985, *Ap. J. Suppl.*, **59**, 513.
Angel, J. R. P., *et al.* 1978, in *Proc. Pittsburgh BL Lacertae Conf.*, ed. A. M. Wolfe (Pittsburgh: University of Pittsburgh), p. 117.
Angel, J. R. P., and Stockman, H. S. 1980, *Ann. Rev. Astr. Ap.*, **18**, 321.
Antonucci, R. R. J. 1984, *Ap. J.*, **278**, 499.
Antonucci, R. R. J., and Miller, J. S. 1985, *Ap. J.*, **297**, 621.
Bailey, J., and Hough, J. H. 1982, *Pub. A.S.P.*, **94**, 618.
Barthel, P. D. 1988, *Ap. J.*, **329**, 1.
Blandford, R. D., and Rees, M. J. 1978, in *Proc. Pittsburgh BL Lacertae Conf.*, ed. A. M. Wolfe (Pittsburgh: University of Pittsburgh), p. 328.
Brindle, C., Hough, J. H., Bailey, J. A., Axon, D. J., and Hyland, A. R. 1986, *M.N.R.A.S.*, **221**, 739.
Browne, I. W. A. 1983, *M.N.R.A.S.*, **204**, 23P.
Browne, I. W. A., and Murphy, D. H. 1987, *M.N.R.A.S.*, **226**, 621.
Burkhead, M. S. 1969, *Pub. A.S.P.*, **81**, 691.
———. 1980, *Pub. A.S.P.*, **92**, 91.
Burkhead, M. S., and Lee, V. J. 1970, *Pub. A.S.P.*, **82**, 1150.
Burkhead, M. S., and Rettig, T. W. 1972, *Pub. A.S.P.*, **84**, 850.
Coleman, H. H., and Shields, G. A. 1990, *Ap. J.*, in press.
Condon, J. J., and Dennison, B. 1978, *Ap. J.*, **224**, 835.
Courvoisier, T. J.-L., Robson, E., Hughes, D., Blecha, A., Bouchet, P., Krisciunas, K., and Schwarz, H. 1988, *Nature*, **335**, 330.
Courvoisier, T. J.-L., *et al.* 1987, *Astr. Ap.*, **176**, 197.
Courvoisier, T. J.-L., and Ulrich, M. H. 1985, *Nature*, **316**, 524.
Cutri, R. M., Wisniewski, W. Z., Reike, G. H., and Lebofsky, M. J. 1985, *Ap. J.*, **296**, 423.
Davis, R. J., Muxlow, T. W. B., and Conway, R. G. 1985, *Nature*, **318**, 343.
de Bruyn, A. G., and Sargent, W. L. W. 1978, *A.J.*, **83**, 1257.
Dolan, J. F., and Tapia, S. 1986, *Pub. A.S.P.*, **98**, 792.
Edelson, R. A., and Malkan, M. A. 1986, *Ap. J.*, **308**, 59.
———. 1987, *Ap. J.*, **323**, 516.
Fillipenko, A. V. 1982, *Pub. A.S.P.*, **94**, 715.
Gear, W. K., *et al.* 1984, *Ap. J.*, **280**, 102.
Impey, C. D. 1987, in *Superluminal Radio Sources*, ed. J. A. Zensus and T. J. Pearson (Cambridge: Cambridge University Press), p. 233.
Impey, C. D., Brand, P. W., Wolstencroft, R. D., and Williams, P. M. 1982, *M.N.R.A.S.*, **209**, 245.
Impey, C. D., and Neugebauer, G. 1988, *A.J.*, **95**, 307.
Impey, C. D., and Tapia, S. 1988, *Ap. J.*, **333**, 666.
———. 1990, *Ap. J.*, submitted.
Jones, T. W., Rudnick, L., Aller, H. D., Aller, M. F., Hodge, P. E., and Feidler, R. L. 1985, *Ap. J.*, **290**, 627.
Kemp, J. C., Reike, G., Lebofsky, M., and Coyne, G. 1977, *Ap. J. (Letters)*, **215**, L107.
Knacke, R. F., Capps, R. W., and Johns, M. 1979, *Nature*, **280**, 215.
Landau, R., *et al.* 1986, *Ap. J.*, **308**, 78.
Landolt, A. 1973, *A.J.*, **78**, 959.
Lee, T. J., Beattie, D. H., Gatley, I., Brand, P. W. J. L., Jones, T., and Hyland, A. R. 1982, *Nature*, **295**, 214.
Liller, W. 1969, *Ap. J.*, **155**, 1113.
Madejski, G. M., and Schwartz, D. A. 1983, *Ap. J.*, **275**, 467.
Malkan, M. A. 1983, *Ap. J.*, **268**, 583.
Malkan, M. A., and Sargent, W. L. W. 1982, *Ap. J.*, **254**, 22.
Moore, R. L., *et al.* 1982, *Ap. J.*, **260**, 415.
Moore, R. L., and Stockman, H. S. 1981, *Ap. J.*, **243**, 60.
———. 1984, *Ap. J.*, **279**, 465.
Neugebauer, G., Oke, J., Becklin, E., and Matthews, K. 1979, *Ap. J.*, **230**, 79.
Orr, M. J., and Browne, I. W. A. 1982, *M.N.R.A.S.*, **200**, 1067.
Peacock, J. A. 1986, Royal Observatory Edinburgh preprint No. 21/86.
Pearson, T. J., and Readhead, A. S. C. 1988, *Ap. J.*, **238**, 114.
Roberts, D. H., and Wardle, J. F. C. 1987, in *Superluminal Radio Sources*, ed. J. A. Zensus and T. J. Pearson (Cambridge: Cambridge University Press), p. 193.
Robson, E. I., Gear, W. K., Brown, L. M. J., Courvoisier, T. J.-L., Smith, M. G., Griffin, M. J., and Blecha, A. 1986, *Nature*, **323**, 134.
Röser, H.-J., and Meisenheimer, K. 1986, *Astr. Ap.*, **154**, 15.
Rudnick, L., Jones, T., Aller, H. D., Aller, M. F., Owen, F., Fiedler, R., Puschell, J., and Bignell, R. 1985, *Ap. J. Suppl.*, **57**, 693.
Rudy, R., Schmidt, G., Stockman, H., and Moore, R. 1983, *Ap. J.*, **271**, 59.
Rusk, R., and Seaquist, E. R. 1985, *A.J.*, **90**, 30.
Sadun, A. C. 1985, *Pub. A.S.P.*, **97**, 395.

Serkowski, K. 1974, in *Methods of Experimental Physics*, Vol. **12**, Part A, ed. N. Carleton (New York: Academic), p. 361.
Serkowski, K., Mathewson, D. S., and Ford, V. L. 1975, *Ap. J.*, **196**, 26.
Simmons, J. F. L., and Stewart, B. G. 1985, *Astr. Ap.*, **142**, 100.
Sitko, M. L., Schmidt, G. D., and Stein, W. A. 1985, *Ap. J. Suppl.*, **59**, 323.
Smith, P. S., Balonek, T. J., Elston, R., and Heckert, P. A. 1987, *Ap. J. Suppl.*, **64**, 459.
Smith, P. S., Balonek, T. J., Heckert, P. A., Elston, R., and Schmidt, G. D. 1985, *A.J.*, **90**, 1184.
Stockman, H. S., Moore, R. L., and Angel, J. R. P. 1984, *Ap. J.*, **279**, 485.
Tapia, S. 1988, Steward Observatory preprint No. 831.
Ulrich, M.-H., Courvoisier, T. J.-L., and Wamsteker, W. 1988, *Astr. Ap.*, **204**, 21.
Unwin, S. C., Cohen, M. H., Biretta, J., Pearson, T. J., Seielstad, G. A., Walker, R. C., Simon, R. S., and Linfield, R. P. 1985, *Ap. J.*, **289**, 109.
Urry, C. M., and Shafer, R. A. 1984, *Ap. J.*, **280**, 569.
Verschuur, G. L. 1970, in *IAU Symposium 39, Interstellar Gas Dynamics*, ed. H. Habing (Dordrecht: Reidel), p. 150.
Wardle, J. F. C., Moore, R. L., and Angel, J. R. P. 1984, *Ap. J.*, **279**, 93.
Warren-Smith, R. F., King, D. J., and Scarrott, S. M. 1984, *M.N.R.A.S.*, **210**, 415.
Webb, W., and Malkan, M. A. 1986, in *Continuum Emission in Active Galactic Nuclei*, ed. M. L. Sitko (Tucson: NOAO), p. 71.
Whiteoak, J. B. 1966, *Zs. Ap.*, **64**, 181.
Wu, C.-C. 1977, *Ap. J.* (*Letters*), **217**, L117.
Young, A. T. 1974, in *Methods of Experimental Physics*, Vol. **12**, Part A, ed. N. Carleton (New York: Academic), p. 123.

C. D. Impey and S. Tapia: Steward Observatory, University of Arizona, Tuscon, AZ 85721

M. A. Malkan: Department of Astronomy, University of California, Los Angeles, CA 90024